Aerosol and Air Quality Research, 17: 1637–1648, 2017

ISSN: 1680-8584 print / 2071-1409 online
doi: 10.4209/aaqr.2016.10.0435

Influences of Copper(II) Chloride Impregnation on Activated Carbon for Low-Concentration Elemental Mercury Adsorption from Simulated Coal Combustion Flue Gas

Cheng-Yen Tsai[1], Chun-Hsiang Chiu[2], Ming-Wei Chuang[3], Hsing-Cheng Hsi[4*]

[1] *Department of Bioenvironmental Systems Engineering, National Taiwan University, Taipei 106, Taiwan*
[2] *Research Center for Environmental Changes, Academia Sinica, Taipei 115, Taiwan*
[3] *Institute of Environmental Engineering and Management, National Taipei University of Technology, Taipei 106, Taiwan*
[4] *Graduate Institute of Environmental Engineering, National Taiwan University, Taipei 106, Taiwan*

ABSTRACT

In this study, the Hg^0 adsorption equilibrium and kinetics of a coconut-shell-based activated carbon impregnated with $CuCl_2$ were examined with respect to their resulting physical and chemical properties. Integrating the results from N_2 adsorption isotherm at 77 K, scanning electron microscopy, elemental analysis, X-ray photoelectron spectroscopy, and Hg^0 adsorption experiments under N_2 and simulated coal-combustion flue gases conditions, it was found that HCl pretreatment could enhance Hg^0 adsorption of crude activated carbon; the Hg^0 adsorption capacities of crude and HCl-pretreated activated carbon under N_2 condition were 95.8 and 225.4 μg g^{-1}, respectively. Additionally, $CuCl_2$ impregnation further increased the adsorption capacity of crude. The Hg^0 adsorption capacity of crude activated carbon with 8% $CuCl_2$ impregnation was 631.1 μg g^{-1}. However, the equilibrium Hg^0 adsorption capacity decreased when Cu loading exceeded 8 wt%, suggesting that adequate forms of surface Cu, O and Cl interacting with flue gas components and Hg^0, as well as the presence of pores with specific size ranges allowing rapid transport of the Hg molecules into the interior of the activated carbon and as energy sinker govern the overall chemisorption process. Pseudo-second-order kinetic model could best describe the adsorption behaviors of tested samples under both test conditions, indicating that Hg^0 adsorbed on the activated carbon surface could be explained by bimolecular reaction mechanisms.

Keywords: Mercury; Adsorbent; Impregnation; $CuCl_2$; Coal-combustion flue gas.

INTRODUCTION

Mercury (Hg) and its compounds emitted from anthropogenic sources, e.g., coal-fired power plants, industrial boilers, waste incinerators, sinters, and cement plants, have tempted substantial attention due to their high toxicity, bioaccumulability, and global transport behaviors in atmosphere (Kumari *et al.*, 2015; Chen *et al.*, 2016; Marusczak *et al.*, 2016; Wang *et al.*, 2016). Coal-fired power plants were reported as the largest single source in most countries in Hg emissions (Pacyna *et al.*, 2010). Hg is present in the coal-combustion flue gases in three major forms, namely, particle-bound (Hg_p), oxidized (Hg^{2+}), and elemental (Hg^0) forms (Hsi *et al.*, 2010; Wilcox *et al.*, 2012). Hg_p and Hg^{2+} can be readily captured by traditional air pollution control devices, such as electrostatic precipitators and wet flue gas desulfurization. In contrast, Hg^0 is highly volatile, insoluble in water, and therefore more difficult to be removed. Furthermore, low-concentration Hg^0 (i.e., at 1–10 ppb_v level) present in coal combustion flue gas streams leads to extreme challenge to control due to mass-transfer limitation. Consequently, novel approaches for low-concentration Hg^0 removal from coal-combustion flue gases have lured marked attention in recent years.

Numerous studies pertaining to develop effective technologies on low-concentration Hg^0 control have been conducted (Li *et al.*, 2015). Using porous materials, especially activated carbons as adsorbents, have been shown as profitable Hg^0 emission control approaches (Lin *et al.*, 2015). The adsorptive efficiency of activated carbon largely depends on the surface and porous characteristics of activated carbon, including surface area, pore volume and size distribution, and surface functionality. The adsorptive environment, namely, flue gas condition, also plays a key role influencing the Hg^0 adsorption effectiveness of activated carbon. For the past decade, sulfur impregnation has been widely reported

* Corresponding author.
Tel.: +886-2-33664374; Fax: +886-2-23928830
E-mail address: hchsi@ntu.edu.tw

to considerably enhance the equilibrium Hg^0 adsorption capacity of activated carbon (Hsi *et al.*, 2001, 2002; Vitolo *et al.*, 2002; Feng *et al.*, 2006; Ho *et al.*, 2008; Hsi *et al.*, 2011, 2012, 2013, 2014). Besides sulfur, activated carbon impregnated with metal salts has demonstrated the competitive adsorption performance to those treated with sulfur. Copper salts, such as $CuCl_2$ and $Cu(NO_3)_2$, have been extensively investigated as impregnation agents since they can not only increase the adsorption capacity of low-concentration Hg^0 but also enhance the oxidation of Hg^0 into water-soluble Hg^{2+} for activated carbon (Williams *et al.*, 1997; Vidic *et al.*, 2001; Kim *et al.*, 2005; Nguyen-Thanh *et al.*, 2005; Lee *et al.*, 2008; Lee *et al.*, 2009a, b, c; Zheng *et al.*, 2012; Li *et al.*, 2013; Du *et al.*, 2014; Liu *et al.*, 2015; Yang *et al.*, 2016a, b, c, d). Lee *et al.* (2009a) suggested that activated carbon containing $CuCl_2$ may possess different sites available for Hg^0 oxidation and Hg adsorption, and the resulted oxidized Hg generated from the reactions between Hg^0 and $CuCl_2$ may be re-adsorbed at other available sites of the $CuCl_2$-treated activated carbon. Li *et al.* (2013) indicated that $CuCl_2$ was the active species responsible for Hg^0 oxidation. In addition, activated carbons with greater chloride contents were found to have larger dynamic adsorption capacities than those with smaller chloride contents (Yang *et al.*, 2016a). The degree of conversion of Hg^0 to Hg^{2+} species was also observed to be directly related to the amount of chloride on the activated carbon (Vidic *et al.*, 2001). Furthermore, Yang *et al.* (2016b) fabricated $CuCl_2$ loaded magnetospheres catalyst; they suggested that there were two different Hg adsorption sites, namely, Cl adsorption and Cu adsorption sites. $Cu(NO_3)_2$ may show competitive Hg^0 adsorption enhancement as $CuCl_2$. However, activated carbon impregnated with $Cu(NO_3)_2$ needed subsequently calcination to increase oxidizing capability of activated carbons. Therefore, $CuCl_2$ was considered a more suitable impregnation agents for enhancing Hg^0 adsorption and oxidation.

Surface oxygenated groups could not only increase Hg^0 adsorption but also enhance the distribution of metal oxides/halides on the surface of activated carbon. Li *et al.* (2003) indicated that oxygenated functionality on the carbon surface, such as lactone and carbonyl groups, could be the active sites for Hg^0 capture. Yang *et al.* (2016d) also reported that the C=O group could be an effective electron acceptor, assisting the electron transfer for Hg^0 oxidation. Tseng *et al.* (2006) further reported that carbonyl groups were generated in activated carbon after HCl treatment; the oxygenated groups could be beneficial for subsequent distribution of CuO on the activated carbon surface. Therefore, to improve the extent of active sites for Hg^0 capture and oxidation, it may be feasible to pretreat activated carbon with acids to produce a variety of surface oxygenated groups acting as bridging sites, followed by metal precursor impregnation.

In the present study, we impregnated a high-quality, coconut-shell-based activated carbon with various amounts of $CuCl_2$ to produce effective adsorbents for removing low-concentration Hg^0 (i.e., in ppb level) from gas streams. Additionally, some activated carbons were pretreated with HCl solution to increase the extent of oxygenated groups on the activated carbon surface followed by subsequent $CuCl_2$ impregnation. The influences of $CuCl_2$ impregnation with and without HCl pretreatment on the physical and chemical properties and Hg^0 adsorption equilibrium/kinetics of resulting samples were then examined and better understood. Results obtained from this study is crucial from practical viewpoint because Taiwan Environmental Protection Administration has announced regulations in October 2013 to limit Hg emissions from coal-fired steam and cogeneration boilers; the Hg emissions should be lowered than 2 and 5 μg Nm^{-3} for new and existing facilities, respectively (Taiwan Environmental Protection Administration, 2014), which addresses the concerns and demands of successful control strategies for Hg emissions from coal-fired power plants.

MATERIALS AND METHODS

Preparation of HCl Pretreated and $CuCl_2$-impregnated Activated Carbon

A high-quality, coconut-shell-based activated carbon with a total surface area of approximately 1113 $m^2\ g^{-1}$ and > 90% microporosity was commercially obtained. The received activated carbon was initially immersed in hot deionized water for 2 h and then washed with cold deionized water several times to remove impurity. After oven-dried at 105°C for 24 h, the cooled sample was ground and passed through a 200-mesh sieve to obtain the homogeneous aliquot sample. The sample was surface-modified with two approaches: (1) HCl pretreatment followed by $CuCl_2$ impregnation, or (2) direct $CuCl_2$ impregnation. For HCl pretreatment, activated carbon sample of 10 g was mechanically stirred in a flask containing 50 mL HCl (37 v/v% from J.T. Baker) for 48 h. The treated activated carbon was separated from acid solution by percolating using a vacuum pump, washed with d.i. water, and then oven-dried at 105°C for 24 h.

The crude and HCl-pretreated activated carbon samples were subsequently impregnated with 2−16 wt% $CuCl_2$ (as Cu, 99.3% purity from J.T. Baker). The samples were immersed in $CuCl_2$ solution at 60−70°C for approximately 6 h that the water was completely vaporized. The resulting samples were then oven-dried at 105°C for 24 h to obtain the final products. The samples are designated as HCAC or CAC for samples with and without HCl pretreatment, respectively, and x wt% indicating the $CuCl_2$ impregnation amount.

Physical and Chemical Characterizations of Activated Carbon

The surface morphology was observed using a scanning electron microscope (Hitachi, model S-4700). Brunauer-Emmett-Teller (BET) specific surface area (S_{BET}), total pore volume (V_{total}) micropore (pore width < 2 nm) surface area (S_{micro}), micropore volume (V_{micro}), and pore-size distribution (PSD) were analyzed using a Quantachrome NOVA 2000e analyzer based on the N_2 adsorption isotherms obtained at 77 K. S_{BET} was determined using the BET equation according to the ASTM D4820-96a method. S_{micro} and V_{micro} were calculated from *t*-plot evaluation based on the Jura-Harkins equation: $t = [13.99/0.0340 - \log(p/p_0)]^{0.5}$ (Lippens *et al.*,

1965). The range of relative pressures chosen for determining S_{micro} and V_{micro} was based on the values of thickness t between 0.45 and 0.8 nm. Micropore size distribution was simulated based on the quenched solid density functional theory (QSDFT). The mesopore size distribution was determined by the Barrett-Joyner-Halenda (BJH) method (Gregg *et al.*, 1982). The chemical composition, including the mass concentration of C and H of samples, was determined by using an elemental analyzer (Thermo Flash EA 1112). Cu mass percent in the sample was verified by acid digestion followed by analysis with flame atomic absorption spectroscopy (FAAS; GBC AA932). The Cl content was determined with an energy dispersive spectrometer (EDS; JEOL JSM-7000F). The O content was estimated based on 100% – (C + H + Cu + Cl)%. The surface functional groups of the samples were further examined by using X-ray photoelectron spectroscopy (XPS; Physical Electronics, model ESCA PHI 1600).

Simulated Coal Combustion Flue Gas Hg^0 Adsorption Test

Detailed descriptions pertaining to experimental apparatus and procedures for Hg^0 adsorption tests have been described elsewhere (Hsi *et al.*, 2011, 2012, 2013; Chiu *et al.*, 2014; Hsi *et al.*, 2014); nevertheless, we present them here again for clarity. The adsorption tests were carried out under two conditions: (1) Hg^0/N_2 condition and (2) simulated coal-combustion flue gas condition containing 6 vol% O_2, 14 vol% CO_2, 10 vol% H_2O, 50 ppm_v HCl, 200 ppm_v SO_2, 200 ppm_v NO, and balance N_2. The simulated coal-combustion flue gas composition was selected to reflect the typical condition of Taiwan's coal-fired power plants, in which low-sulfur bituminous and sub-bituminous coal blends are generally fired. The gas flow rate was controlled at 1.2 L min^{-1} with a Hg^0 concentration at 82 μg Nm^{-3} (i.e., 10 ppb_v). Hg^0 was generated with a certificated Hg^0 permeation tube (VICI Metronics) at 70 ± 0.1°C to ensure a constant Hg^0 diffusion rate. The Hg^0-containing gas homogeneously mixed with N_2 or simulated coal-combustion flue gas was passed through a temperature-controlled fixed-bed column (0.5-in i.d.) containing a 10 mg sample mixed with 3 g quartz sand. The column length of the sample/sand mixture was approximately 5 cm and the duration for gas stream to pass the mixture was around 0.3 s. The temperature of fixed-bed column and heated Teflon tubes was controlled at 150°C and 110−130°C respectively to avoid moisture condensation. The effluent gas from the fixed-bed column flowed through the heated lines to the first impinger containing 20% $SnCl_{2(aq)}$ that reduces any oxidized Hg compounds to Hg^0 followed by the second impinger containing 12% $Na_2CO_{3(aq)}$ to remove the acidic components. The gas then flowed through a Nefion tube to remove H_2O and protect the downstream detector. The gas finally flowed through a gold amalgamation system (Brooks Rand model AC-01) where the Hg^0 in the gas was adsorbed. Hg^0 concentrated on the gold was subsequently desorbed at temperature > 400°C, and was sent as a concentrated Hg^0 stream to a cold-vapor atomic fluorescence spectrophotometer (CVAFS; Brooks Rand Lab Model III) for analysis. The test was stopped when 100% breakthrough reached, or conducted for up to 975 min. Hg^0 adsorption capacities, presented as g-Hg^0 g^{-1} adsorbent at given time, were determined by summing the mass of Hg^0 removed from the gas stream on the basis of the obtained breakthrough curves and then dividing by the mass of the adsorbent in the adsorption bed:

$$\frac{m_i}{m_{adsorbent}} = \sum_{t=0}^{t'} \frac{\left(C_{i,in} - C_{i,out}\right) \times Q_g}{m_{adsorbent}} \Delta t \quad (1)$$

where m_i is the mass of adsorbed Hg, $m_{adsorbent}$ is the total mass of adsorbent, t' is the adsorption time, $C_{i,in}$ is the inlet Hg concentration, $C_{i,out}$ is the outlet Hg concentration at time t, Q_g is the gas flow rate, and t is the time interval during the breakthrough test.

RESULTS AND DISCUSSION

Properties of Adsorbents Prior to and After $CuCl_2$ Impregnation

The surface morphology of activated carbon before and after $CuCl_2$ impregnation is shown in Fig. 1. Dramatic changes on the surface shape and roughness of the samples after HCl pretreatment and $CuCl_2$ impregnation were not observed, implying that the distribution of $CuCl_2$ on activated carbon surface was fairly uniform.

The BET surface area, total pore volume, micropore surface area, and micropore volume of samples are shown in Table 1. Generally, $CuCl_2$ impregnation decreased the surface area and pore volume of all resulting activated carbons. The S_{micro} of crude CAC was 1113 ± 117 m^2 g^{-1} and S_{BET} was 1168 ± 77.0 m^2 g^{-1}. The calculated S_{micro}/S_{BET}, namely 95.2 ± 3.7%, suggests that crude CAC contains a marked amount of micropores. Additionally, pronounced difference in the S_{micro}, S_{BET}, and S_{micro}/S_{BET} between crude CAC and HCAC samples was not observed, indicating that the surface area and pore structure of activated carbon are less affected by acid treatment, or in other words, by the introduction of additional oxygenated groups. In contrast, pore blockage influencing surface area and pore volume by $CuCl_2$ impregnation was found; the extent of influence greatly depended on the amount of impregnated $CuCl_2$. For instance, after 16 wt% $CuCl_2$ impregnation, the S_{micro} dropped to 799.3 ± 35.6 m^2 g^{-1} and the S_{BET} was about 901.3 ± 24.5 m^2 g^{-1}. The V_{micro} also reduced from 0.58 ± 0.02 cm^3 g^{-1} (crude CAC) to 0.42 ± 0.01 cm^3 g^{-1} (CAC 16%) and the V_{total} decreased from 0.65 ± 0.12 cm^3 g^{-1} (crude CAC) to 0.52 ± 0.02 cm^3 g^{-1} (CAC 16%). HCAC 2%, 8% and 16% samples also showed a similar trend of physical property changes with CAC series samples after $CuCl_2$ impregnation. It is important to note that, the S_{micro}/S_{BET} had no significant variation after $CuCl_2$ impregnation, suggesting that $CuCl_2$ uniformly blocked not only micropores but also macropores and mesopores of activated carbon.

The physical property changes due to surface modification could also be observed by the PSD simulation results, which are illustrated in Fig. 2. Based on the results in Table 1, all

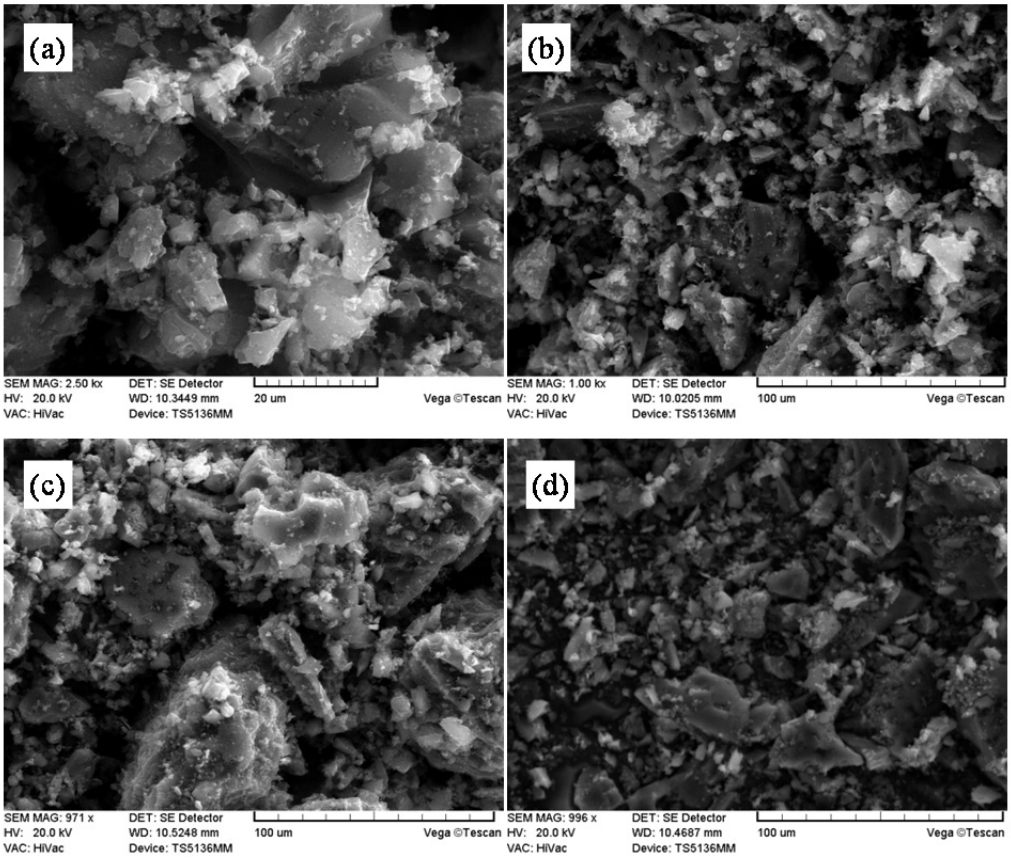

Fig. 1. SEM images of (a) crude CAC, (b) CAC 16%, (c) crude HCAC, and (d) HCAC 16%.

Table 1. Total/micropore area and volume and microporosity of activated carbon samples prior to and after HCl pretreatment and $CuCl_2$ impregnation.

Sample	S_{micro} ($m^2\ g^{-1}$)	S_{BET} ($m^2\ g^{-1}$)	S_{micro}/S_{BET} (%)	V_{micro} ($cm^3\ g^{-1}$)	V_{total} ($cm^3\ g^{-1}$)	V_{micro}/V_{total} (%)
CAC	1113 ± 117	1168 ± 77.0	95.2 ± 3.7	0.58 ± 0.02	0.65 ± 0.12	90.4 ± 6.2
CAC 2%	800.1 ± 96.4	856.8 ± 107	93.4 ± 2.2	0.42 ± 0.03	0.45 ± 0.02	88.6 ± 4.1
CAC 8%	889.4 ± 111	951.5 ± 72.7	93.3 ± 4.6	0.46 ± 0.03	0.53 ± 0.01	87.3 ± 7.5
CAC 16%	799.3 ± 35.6	901.3 ± 24.5	88.7 ± 1.7	0.42 ± 0.01	0.52 ± 0.02	79.8 ± 1.6
HCAC	1049 ± 158	1135 ± 103	92.2 ± 5.6	0.54 ± 0.06	0.63 ± 0.00	86.0 ± 8.9
HCAC 2%	850.5 ± 158	941.2 ± 33.9	90.4 ± 3.0	0.44 ± 0.02	0.53 ± 0.05	83.2 ± 2.9
HCAC 8%	849.6 ± 96.2	908.6 ± 31.1	93.4 ± 7.4	0.44 ± 0.03	0.50 ± 0.04	88.3 ± 12.8
HCAC 16%	814.1 ± 269	922.8 ± 265	87.7 ± 4.0	0.42 ± 0.12	0.53 ± 0.11	79.2 ± 5.1

test samples can be classified as microporous activated carbons. Both crude CAC and HCAC samples had a unimodal micropore size distribution with a peak at around 0.6−0.8 nm (Fig. 2(a)); peak shift after HCl pretreatment was not found. In contrast, $CuCl_2$ impregnation caused significant changes in PSDs for both CAC and HCAC samples. Notably, the change in peak volume, not in peak position was markedly influenced by the impregnation content. This observation supports that the decrease in micropore volume is mainly due to pore blockage, not pore shrinkage. Fig. 2(b) further shows that $CuCl_2$ impregnation had no significant effects on altering the mesopore structure of CAC and HCAC, which occupied < 10% of the total porosity.

Table 2 lists the results of element analyses for the activated carbon prior to and after HCl pretreatment and $CuCl_2$ impregnation with various concentrations. C and O were the main elements in CAC and HCAC samples. HCl pretreatment enhanced the balanced O content of crude activated carbon from 4.39 to 8.02 wt%, as well as increasing the Cl content to 0.34 wt%. $CuCl_2$ impregnation substantially increased the total Cu amount based on acid digestion/FAAS analysis, which increased with elevating impregnated $CuCl_2$ content. Cl content also increased with increasing $CuCl_2$ impregnation amount based on EDS analysis. However, the increase in Cl extent was much smaller than the increase in Cu content, which may be due to vaporization of Cl compounds during impregnation and oven-drying process.

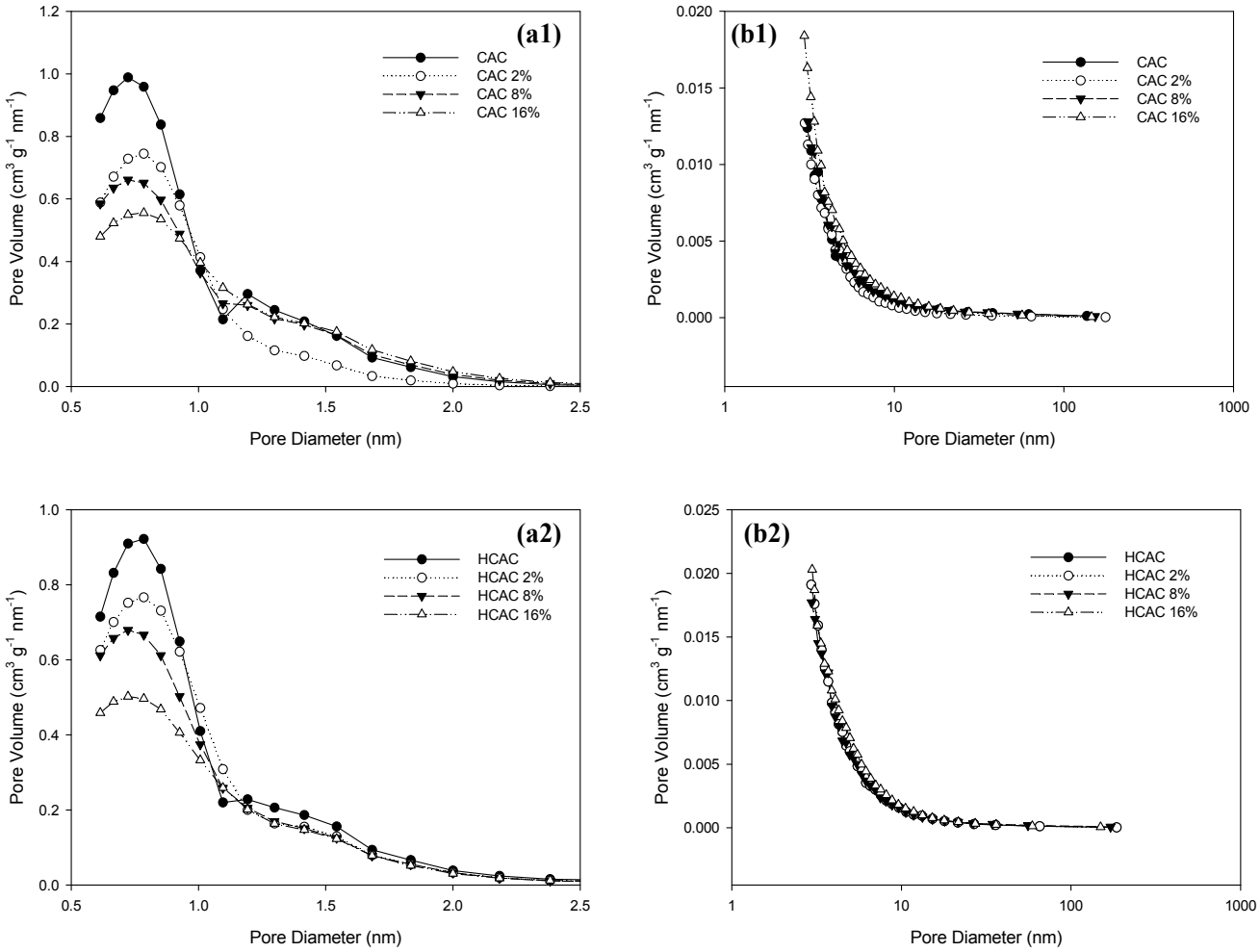

Fig. 2. (a) Micropore and (b) mesopore size distributions of crude and $CuCl_2$-impregnated (1) CAC and (2) HCAC.

Table 2. Chemical composition of activated carbon samples prior to and after HCl pretreatment and $CuCl_2$ impregnation.

Sample	C (wt%)	H (wt%)	Cu (wt%) [a]	Cl (wt%) [b]	O (wt%) [c]
CAC	94.0	1.61	0.00	0.00	4.39
CAC 2%	93.0	1.64	1.38	0.24	3.74
CAC 8%	83.7	2.16	6.79	0.57	6.78
CAC 16%	76.6	2.24	13.0	1.18	6.98
HCAC	89.6	2.04	0.00	0.34	8.02
HCAC 2%	89.2	1.60	1.64	0.41	7.15
HCAC 8%	86.7	1.68	5.85	0.79	4.98
HCAC 16%	80.2	1.43	13.8	3.29	1.28

[a] Cu content was determined by acid digestion followed by FAAS analysis.
[b] Cl content was determined by EDS analysis.
[c] balanced O content = 100% – (C + H + Cu + Cl)%.

In contrast, the C contents of samples were shown to correspondingly decrease with increasing the Cu contents. For example, the C and Cu amounts of CAC 2% were 93.0 and 1.38 wt%, respectively, but CAC 16% had C content of 76.6 wt% and Cu content of 13.0 wt%. A similar tendency was also observed in $CuCl_2$-impregnated HCACs. These experimental results support our previous observation that the impregnated agents could be doped into the porous adsorbents by means of surface coverage or pore filling, or by both mechanisms at the same time (Hsi *et al.*, 2002, 2011, 2012, 2013, 2014).

XPS analysis verified that C/O and C/O/Cl were on the surface of crude CAC prior to and after $CuCl_2$ impregnation, respectively (Fig. 3). C-functional groups including graphitic structure (C-C and C-H bonding; 284.4–284.6 eV), hydroxyl (C-OH bonding; 286.1–286.5 eV), carbonyl (C=O bonding; 287.7–288.2 eV), carboxyl groups (C-COOH bonding; 289.3–289.9 eV), and π-electron resonance (292.7–294.2 eV)

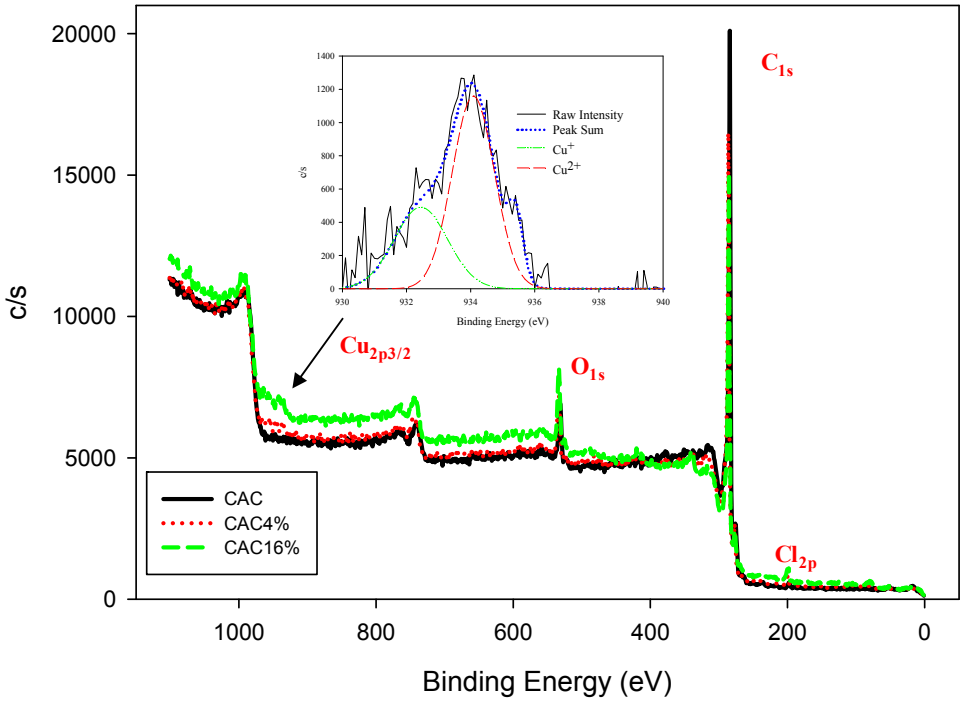

Fig. 3. XPS spectra of crude, 4% and 16% $CuCl_2$-impregnated CAC samples and deconvoluted $Cu_{2p3/2}$ curves for CAC 16% sample.

were further deconvoluted and their corresponding percentages of total C_{1s} peak area were then determined. The relative potions of C_{1s} peak area for crude CAC were 73.6% for graphite, 11.0% for hydroxyl, 5.55% for carbonyl, 9.32% for carboxyl, and 0.58% for π-electron resonance, respectively. After $CuCl_2$ impregnation, the graphitic content of activated carbon samples decreased. For example, the relative potions of C_{1s} for CAC 16% were 66.6% (graphite), 9.41% (hydroxyl), 19.3% (carbonyl), 4.18% (carboxyl), and 0.61% (π-electron resonance), respectively. These deconvolution results suggest that carbonyl content could increase with elevating $CuCl_2$ impregnation content. It is important to note that lactone and carbonyl functionality groups have been suggested to promote Hg adsorption through chemisorption based on the bonding energies calculated by density functional theory (Padak *et al.*, 2006). Furthermore, Skodras *et al.* (2007) reported that oxygen functional groups can facilitate the electron-transfer process and Hg^0 oxidation on the carbon surface and act as potential adsorption centers of Hg^0. Fig. 3 also illustrates that $Cu_{2p3/2}$ XPS spectrum obtained from the CAC 16% sample could be deconvoluted into two peaks within 932.0–934.2 eV, including Cu^+ (31.6% of total Cu peak area with 932.0–932.8 eV) and Cu^{2+} (68.4% of total Cu peak area within 932.9–934.2 eV). Cl_{2p} peak at 198.7 eV also indicated the presence of metal chloride after $CuCl_2$ impregnation.

Hg^0 Removal Performance under N_2 and Simulation Flue Gas Conditions

The Hg^0 adsorption capacities of the crude, HCl-pretreated, and $CuCl_2$-impregnated samples are illustrated in Fig. 4. The crude CAC and HCAC adsorbents, in general, demonstrated smaller adsorption capacities than the $CuCl_2$-impregnated samples under N_2 condition (Figs. 4(a) and (b)). For instance, the equilibrium Hg^0 adsorption capacity of crude CAC was 95.8 μg g^{-1}, but that for $CuCl_2$-impregnated samples, such as CAC 2% and CAC 16%, was 417.2 and 435.8 μg g^{-1}, respectively (Fig. 4(a)). In addition, the Hg^0 adsorption capacity of CAC 8% achieved 631.1 μg g^{-1}, which was the greatest adsorption performance compared to other crude and $CuCl_2$-impregnated CACs. These adsorption results may stem from two reasons: first, the S_{BET} of CAC 8% is greater than those of CAC 2% and CAC 16% samples and consequently CAC 8% has more surface area containing active sites for Hg^0 adsorption. Second, although the S_{BET} of crude CAC is greater than that of CAC 8%, crude CAC lacks Hg^0 adsorption sites that were provided by the impregnated $CuCl_2$. Fig. 4(b) illustrates the Hg^0 adsorption results for HCAC series samples under N_2 condition. The Hg^0 adsorption capacity of HCAC 8% was 479.8 μg g^{-1}, which was larger than 458.4 μg g^{-1} (HCAC 16%), 332.6 μg g^{-1} (HCAC 2%), and 225.4 μg g^{-1} (crude HCAC). Notably, the crude HCAC sample (225.4 μg g^{-1}) had a greater Hg^0 adsorption capacity than crude CAC (95.8 μg g^{-1}), indicating that oxygenated groups and remained Cl introduced by HCl pretreatment could enhance Hg^0 adsorption of activated carbon without $CuCl_2$ impregnation. After $CuCl_2$ impregnation, HCAC series samples did not show a significant increase in Hg^0 capture. Notably, S_{BET} and Cu amount of HCAC 8% were smaller than those of CAC 8% sample, which could be one of the reasons that HCAC 8% had a lower Hg^0 adsorption capacity than CAC 8%.

The Hg^0 adsorption results obtained under N_2 condition for $CuCl_2$-impregnated activated carbons indicate the

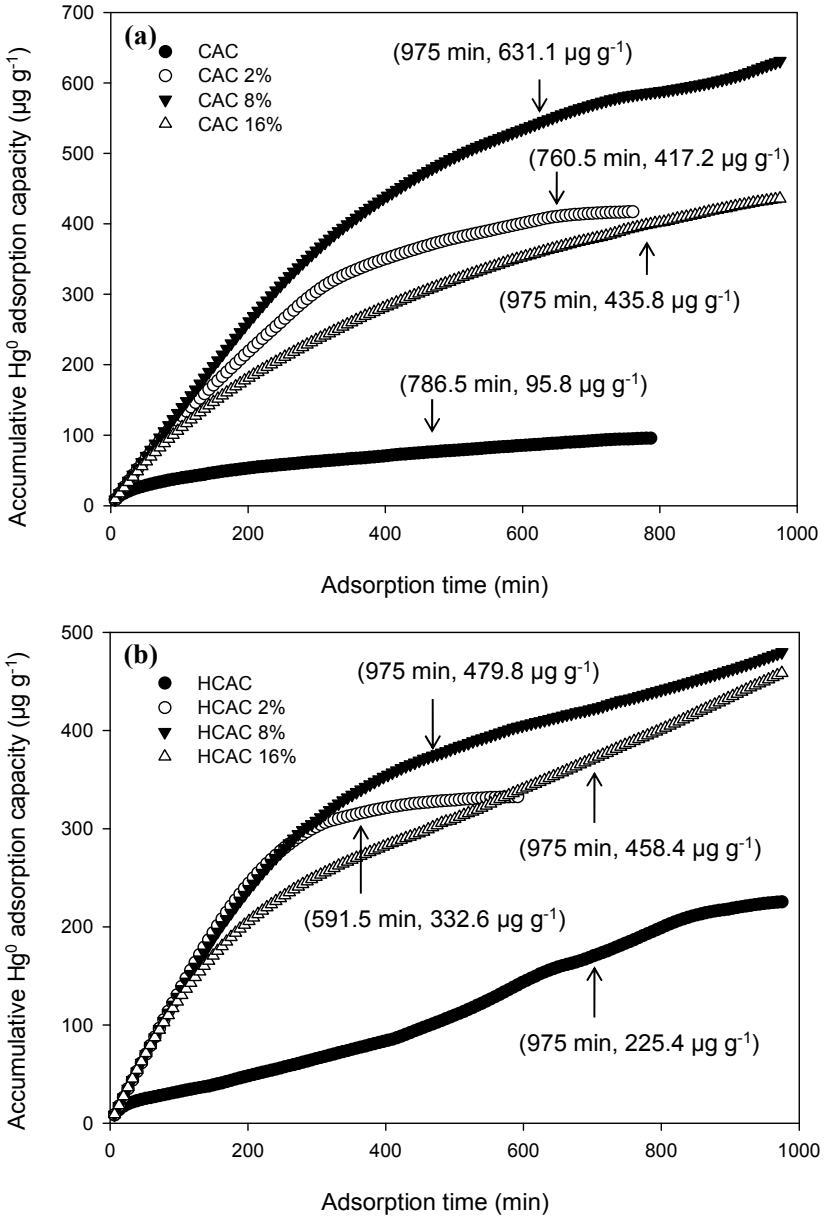

Fig. 4. Accumulative Hg^0 adsorption capacity of (a) CAC, (b) HCAC under N_2 condition.

importance of $CuCl_2$ impregnation in Hg^0 adsorption. The impregnated $CuCl_2$, expected to be mainly in Cl-Cu-Cl form or Cl-Cu-O form by interacting with carbon surface, could be active adsorption sites for capture of Hg^0 via chemisorption. Notably, Yang *et al.* (2016b) and Liu *et al.* (2015) have reported that different Cu loading on the sorbent surface caused various Cu coordination; isolated Cu^{2+} at low Cu loading and associated Cu^{2+} at high Cu loading ions existed in chlorine-free and chlorine-enriched situations, respectively. The active adsorption sites for Hg^0 were typically created by the chlorine-enriched coordination, not chlorine-free. Therefore, in our study, we expected that when $CuCl_2$ impregnation amount was increased, the chlorine-enriched coordination on the impregnated CAC dominated and enhanced the Hg^0 adsorption. Nevertheless, it is important to address that a large amount of $CuCl_2$ in activated carbon does not guarantee great Hg^0 adsorption performance. For instance, CAC 16% and HCAC 16% had a Cu content of approximately 13 wt% (Table 2) but the Hg^0 adsorption capacities are smaller than those of CAC 8% and HCAC 8%. The microporous structure is shown to be retained after $CuCl_2$ impregnation, indicating that the extent of pore surface area/volume is not the limiting factor in Hg^0 capture. In contrast, the decrease in microporosity, namely, the decrease in certain "key" micropores with specific pore sizes, may play a more important role in adsorption. In addition, a high $CuCl_2$ impregnation amount may also result in hindering effects on inherent, effective surface functional groups (such as inherent and introduced oxygenated groups), which could be another cause resulting in the smaller Hg^0 adsorption.

Figs. 5(a) and 5(b) show the Hg^0 adsorption involving

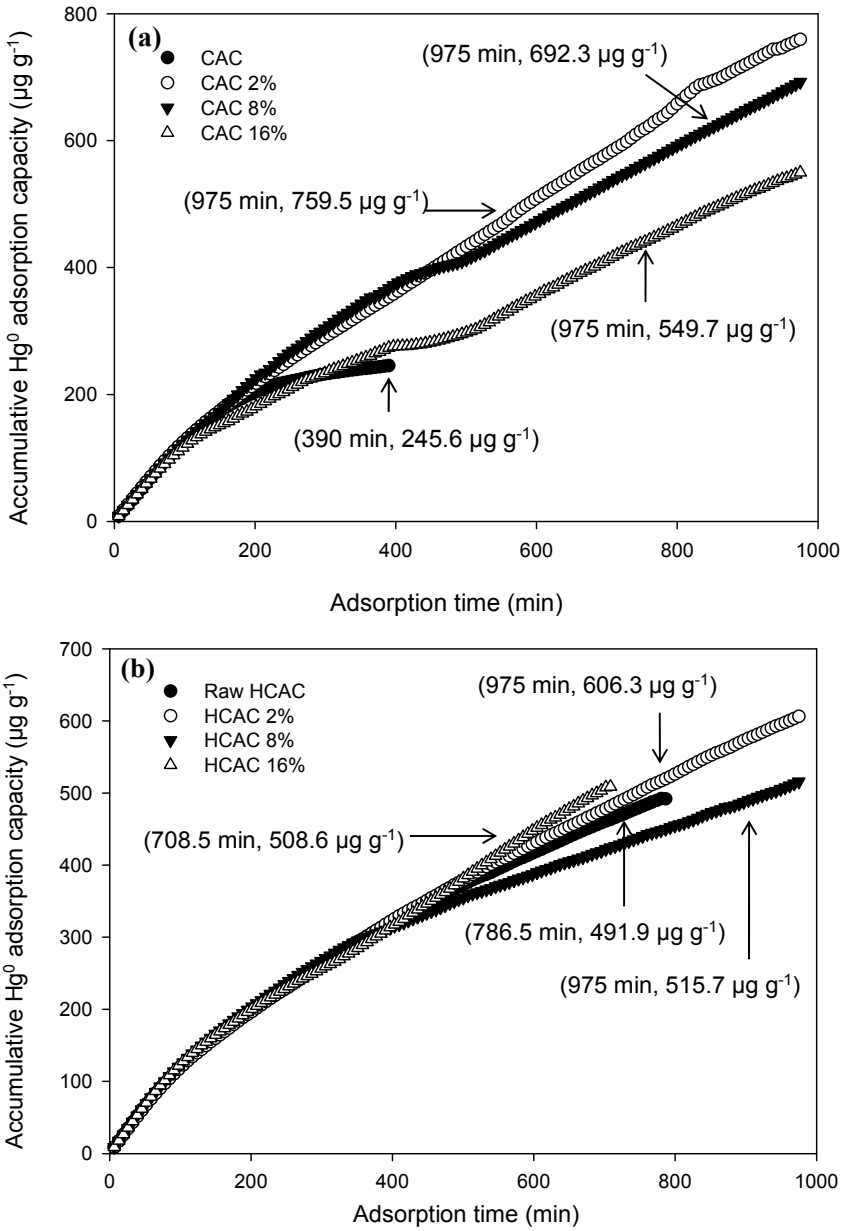

Fig. 5. Accumulative Hg^0 adsorption capacity of (a) CAC and (b) HCAC under simulated flue gas condition.

crude and $CuCl_2$-impregnated CAC and HCAC samples under simulated coal-combustion flue gas condition. Similar to those observed under N_2 condition, the crude activated carbon without impregnated with $CuCl_2$ had smaller adsorption capacities (245.6 μg g^{-1} for CAC and 491.9 μg g^{-1} for HCAC, respectively) than $CuCl_2$-impregnated samples. However, the effects of $CuCl_2$ impregnation for activated carbons under these two test conditions are dissimilar. Under the flue gas condition, CAC 2% and HCAC 2% samples had the largest Hg^0 adsorption capacities of 759.5 and 606.3 μg g^{-1} respectively compared to the other samples. Additionally, the Hg^0 adsorption capacities of samples under the flue gas condition were in general greater than those under N_2 condition, suggesting the enhancing effects of flue gas components, such as SO_2, HCl, and O_2, on Hg^0 adsorption (Hsi *et al.*, 2012). These observations again support that the total surface area and total $CuCl_2$ amount of adsorbents could markedly influence Hg^0 adsorption but not the only determining factors on both Hg^0 adsorption equilibrium and kinetics, which was implied by the slope of the breakthrough curves and adsorption duration. Specific forms of Cu and oxygenated groups playing as catalytic and adsorption sites and pores with specific size ranges allowing rapid transport of the Hg molecules into the interior of the activated carbon and as energy sinker govern the adsorption process (Hsi *et al.*, 2002, 2011, 2013).

Kinetic Analysis of Hg^0 Adsorption on Crude and $CuCl_2$-impregnated Activated Carbons

To further understand the mechanisms of Hg^0 adsorption on crude and $CuCl_2$-impregnated adsorbents and the conceivable rate limiting steps, kinetic models were employed to the

adsorption results from Hg^0 adsorption breakthrough tests. Because various functionalities including oxygen, chloride, and copper groups on the carbon surface may cause various types of adsorbent-adsorbate interactions, a lumped and simplified kinetic analysis is a practical approach from a system design viewpoint (Juang *et al.*, 2000; Yang *et al.*, 2005; Hsi *et al.*, 2011, 2012). The pseudo-first and second-order kinetic models assuming that adsorption is resolved by pseudo chemical reaction processes were chosen and the adsorption rates can be determined respectively by the following first-order and second-order reaction rate equations:

$$dq_t/dt = k_1(q_e - q_t) \quad (2)$$

$$dq_t/dt = k_2(q_e - q_t)^2 \quad (3)$$

where q_t (μg g^{-1}) is the Hg^0 adsorption capacity at time t (min), q_e (μg g^{-1}) is the equilibrium Hg^0 adsorption capacity, and k_1 (min^{-1}) and k_2 (g μg^{-1} min^{-1}) are the pseudo first and second-order rate constants, respectively. These equations represent initial value problems and have analytical solution when combined with the conditions $q_t = 0$ at t = 0 and $q_t = q_t$ at $t = t$. The solutions for Eqs. (2) and (3) respectively are expressed as:

$$\ln(q_e - q_t) = \ln(q_e) - k_1 t \quad (4)$$

$$t/qt = 1/(k_2 q_e^2) + t/q_e \quad (5)$$

For the pseudo-first-order kinetic model, a linear driving force similarity is achieved when the driving force is depicted as a concentration dissimilarity (Ho *et al.*, 1998). Some researchers have thus used the pseudo-first-order simulation to describe reaction, adsorption, and unsteady state diffusion. In contrast, when the adsorption seems to follow pseudo-second-order kinetic model and the rate is mostly concluded by chemisorption, the model on the basis of Langmuir-type second-order mass action rate expression could better address the adsorption characteristics (Skodras *et al.*, 2008). Moreover, the chemisorption occurring on a strong heterogeneous surface can also be modelled by the Elovich equation, which is given by

$$(dq_t/dt) = \alpha \exp(-\beta q_t) \quad (6)$$

Given that $q_t = q_t$ at t = t and qt = 0 at t = 0, the integrated form of Eq. (7) is

$$q_t = (1/\beta)\ln(t + t_0) - (1/\beta)\ln t_0 \quad (7)$$

where $t_0 = 1/\alpha\beta$. If $t >> t_0$, Eq. (7) can be simplified as

$$q_t = (1/\beta)\ln(\alpha\beta) + (1/\beta)\ln t \quad (8)$$

The modeling kinetic constants, R^2 values, and sum of squared error (SSE) using pseudo first-order, pseudo second-order, and Elovich equations for simulation are shown in Table 3 and Fig. 6. R^2 value of pseudo first-order and pseudo second-order were 0.726−0.935 and 0.849–0.997,

Table 3. Kinetic constants, R^2 and sum of squared values for pseudo-first-order, pseudo-second-order, and Elovich simulations.

Sample		Pseudo-first-order simulation			Pseudo-second-order simulation			Elovich simulation		
		k_1 (min^{-1})	R_1^2	*SSE*	k_2 (g μg^{-1} min^{-1})	R_2^2	*SSE*	R_3^2	α	β
CAC	N_2 condition	4.84×10^{-4}	0.816	1.21×10^{4}	4.85×10^{-5}	0.972	1.20×10^{3}	0.941	1.279	5.41×10^{-2}
CAC 2%		7.37×10^{-3}	0.872	8.42×10^{5}	3.89×10^{-6}	0.975	1.27×10^{4}	0.886	4.018	9.56×10^{-3}
CAC 8%		3.92×10^{-3}	0.935	3.96×10^{5}	1.09×10^{-6}	0.954	3.82×10^{4}	0.918	5.684	5.18×10^{-3}
CAC 16%		3.92×10^{-3}	0.867	3.72×10^{5}	3.26×10^{-6}	0.997	7.00×10^{2}	0.929	3.332	9.44×10^{-3}
HCAC		3.92×10^{-3}	0.726	7.74×10^{5}	4.22×10^{-7}	0.880	1.44×10^{4}	0.728	1.199	1.60×10^{-2}
HCAC 2%		1.11×10^{-2}	0.925	6.64×10^{5}	5.37×10^{-6}	0.935	4.35×10^{5}	0.945	9.678	7.86×10^{-3}
HCAC 8%		3.69×10^{-3}	0.909	5.43×10^{4}	3.90×10^{-6}	0.989	1.09×10^{4}	0.962	4.920	7.91×10^{-3}
HCAC 16%		3.22×10^{-3}	0.832	2.35×10^{5}	3.64×10^{-6}	0.977	2.36×10^{4}	0.934	4.130	8.84×10^{-3}
CAC	Flue gas condition	1.36×10^{-2}	0.918	3.34×10^{5}	4.81×10^{-6}	0.939	1.47×10^{4}	0.950	9.961	7.09×10^{-3}
CAC 2%		3.46×10^{-3}	0.788	1.92×10^{6}	4.89×10^{-7}	0.876	1.68×10^{4}	0.832	3.582	6.02×10^{-3}
CAC 8%		3.22×10^{-3}	0.812	1.68×10^{6}	5.67×10^{-7}	0.965	4.70×10^{4}	0.874	5.341	4.55×10^{-3}
CAC 16%		2.99×10^{-3}	0.779	1.52×10^{6}	1.08×10^{-6}	0.849	9.71×10^{4}	0.840	4.315	6.01×10^{-3}
HCAC		4.61×10^{-3}	0.782	6.45×10^{5}	1.93×10^{-6}	0.985	4.67×10^{3}	0.895	3.659	8.54×10^{-3}
HCAC 2%		3.22×10^{-3}	0.826	1.51×10^{6}	7.03×10^{-7}	0.958	4.91×10^{4}	0.872	4.737	5.22×10^{-3}
HCAC 8%		3.22×10^{-3}	0.863	2.53×10^{5}	2.67×10^{-7}	0.991	2.09×10^{3}	0.922	3.584	8.56×10^{-3}
HCAC 16%		3.46×10^{-3}	0.838	8.17×10^{5}	1.08×10^{-6}	0.918	1.92×10^{4}	0.859	2.980	8.10×10^{-3}

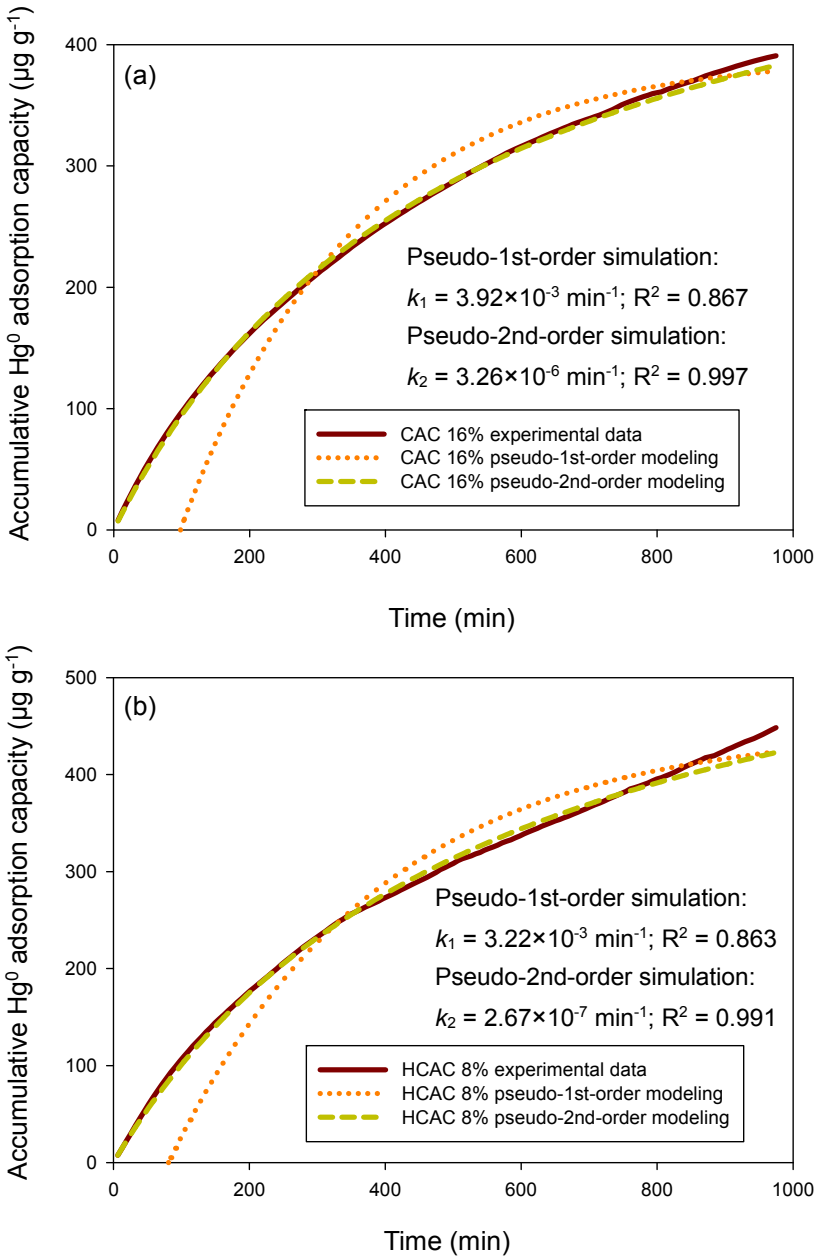

Fig. 6. Comparison of pseudo-first-order and pseudo-second-order kinetic simulations for (a) N_2 condition and (b) simulated flue gas condition.

respectively. The R^2 value of Elovich equation was within 0.728−0.962. Therefore, pseudo-second-order equation was demonstrated to best describe the Hg^0 adsorption kinetics over the entire fractional approach to equilibrium for all tested samples, which was consistent with those shown in (Skodras *et al.*, 2008) and implied the nature of a chemisorption process. These simulation results suggest that Hg^0 adsorption on $CuCl_2$-impregnated adsorbents appear to occur in bimolecular form, namely, two active sites are occupied to capture one molecule of Hg^0. The active sites could be supplied by $CuCl_2$ impregnation, including both Cu and Cl functionality, or provided by other surface groups including inherent and additional oxygenated groups resulted from HCl pretreatment.

CONCLUSION

Effective Hg adsorbents via $CuCl_2$ impregnation on activated carbons to enhance equilibrium Hg^0 adsorption were successfully prepared. Overall, $CuCl_2$ impregnation altered the physical and chemical properties of activated carbons, increasing the total Cu and Cl content and lowering the surface area and pore volume of all prepared samples. SEM images suggested that the surface morphology of crude and treated activated carbons was similar. Elemental and XPS analyses not only verified the increase in O content after HCl pretreatment and the presence of Cu in activated carbons after $CuCl_2$ impregnation, but also showed that Cu was present in both Cu^{2+} and Cu^{+} forms.

CAC and HCAC samples after 2 wt% and 8 wt% $CuCl_2$ impregnation possessed the largest Hg^0 adsorption capacity under N_2 and simulated coal combustion flue gas conditions, respectively. Results from this study support our earlier finding that a large amount of $CuCl_2$ in activated carbon does not necessarily guarantee great Hg^0 adsorption performance. Furthermore, total pore surface area/volume is not the limiting factor in Hg^0 capture. The decrease in certain key microporosity with specific pore sizes may play a more critical role in Hg^0 adsorption. Specific forms of Cu and oxygenated groups and the presence of Cl playing as catalytic and adsorption sites, adequate interaction of surface functionality, flue gas components and Hg^0, and pores with specific size ranges allowing rapid transport of the Hg molecules into the interior of the activated carbon and as energy sinker govern the chemical adsorption process.

ACKNOWLEDGEMENTS

This work was financially supported by the Ministry of Science and Technology, Taiwan under Grant no. 97-2221-E-327-006-MY3

REFERENCES

Chen, W.K., Li, T.C., Sheu, G.R., Lin, N.H., Chen, L.Y. and Yuan, C.S. (2016). Correlation analysis, transportation mode of atmospheric mercury and criteria air pollutants, with meteorological parameters at two remote sites of mountain and offshore island in Asia. *Aerosol Air Qual. Res.* 16: 2692–2705.

Chiu, C.H., Hsi, H.C. and Lin, C.C. (2014). Control of mercury emissions from coal-combustion flue gases using $CuCl_2$-modified zeolite and evaluating the cobenefit effects on SO_2 and NO removal. *Fuel Process. Technol*. 126: 138–144.

Chiu, C.H., Lin, H.P., Kuo, T.H., Chen, S.S., Su, K.H. and Hsi, H.C. (2015). Simultaneous control of elemental mercury/sulfur dioxide/nitrogen monoxide from coal-fired flue gases with metal oxide-impregnated activated carbon. *Aerosol Air Qual. Res.* 15: 2094–2103.

Du, W., Yin, L., Zhuo, Y., Xu, Q., Zhang, L. and Chen, C. (2014). Catalytic oxidation and adsorption of elemental mercury over $CuCl_2$-impregnated sorbents. *Ind. Eng. Chem. Res.* 53: 582–591.

Feng, W., Borguet, E. and Vidic, R.D. (2006). Sulfurization of carbon surface for vapor phase mercury removal – I: Effect of temperature and sulfurization protocol. *Carbon* 44: 2990–2997.

Gregg, S.J. and Sing, K.S.W. (1982). *Adsorption, Surface Area and Porosity*, 2nd ed. Academic Press, London.

Ho, T.C., Shetty, S., Chu, H.W., Lin C.J. and Hopper, J.R. (2008). Simulation of mercury emission control by activated carbon under confined-bed operations. *Powder Technol*. 180: 332–338.

Ho, Y.S. and McKay, G. (1998). A comparison of chemisorption kinetic models applied to pollutant removal on various sorbents. *Process Saf. Environ. Prot.* 76: 332–340.

Hsi, H.C., Rood, M.J., Rostam-Abadi, M., Chen, S. and Chang, R. (2001). Effects of sulfur impregnation temperature on the properties and mercury adsorption capacities of activated carbon fibers (ACFs). *Environ. Sci. Technol.* 35: 2785–2791.

Hsi, H.C., Rood, M.J., Rostam-Abadi, M., Chen, S. and Chang, R. (2002). Mercury adsorption properties of sulfur-impregnated adsorbents. *J. Environ. Eng.* 128: 1080–1089.

Hsi, H.C., Lee, H.H., Hwang, J.F. and Chen, W. (2010). Mercury speciation and distribution in a 660-megawatt utility boiler in Taiwan firing bituminous coals. *J. Air Waste Manage. Assoc.* 60: 514–522.

Hsi, H.C., Tsai, C.Y., Kuo, T.H. and Chiang, C.S. (2011). Development of low-concentration mercury adsorbents from biohydrogen-generation agricultural residues using sulfur impregnation. *Bioresour. Technol.* 102: 7470–7477.

Hsi, H.C. and Chen, C.T. (2012). Influences of acidic/oxidizing gases on elemental mercury adsorption equilibrium and kinetics of sulfur-impregnated activated carbon. *Fuel* 98: 229–235.

Hsi, H.C., Rood, M.J., Rostam-Abadi, M. and Chang, Y.M. (2013). Effects of sulfur, nitric acid, and thermal treatments on the properties and mercury adsorption of activated carbons from bituminous coals. *Aerosol Air Qual. Res.* 13: 730–738.

Hsi, H.C., Tsai, C.Y. and Lin, K.J. (2014). Impact of surface functional groups, water vapor, and flue gas components on mercury adsorption and oxidation by sulfur-impregnated activated carbons. *Energy Fuels* 28: 3300–3309.

Juang, R.S., Wu, F.C. and Tseng, R.L. (2000). Mechanism of adsorption of dyes and phenols from water using activated carbons prepared from plum kernels. *J. Colloid Interface Sci.* 227: 437–444.

Kim, D.J. and Yie, J.E. (2005). Role of copper chloride on the surface of activated carbon in adsorption of methyl mercaptan. *J. Colloid Interface Sci.* 283: 311–315.

Kumari, A., Kumar, B., Manzoor, S. and Kulshrestha, U. (2015). Status of atmospheric mercury research in South Asia: A review. *Aerosol Air Qual. Res.* 15: 1092–1109.

Lee, S.S., Lee, J.Y. and Keener, T.C. (2008). Novel sorbents for mercury emissions control from coal-fired power plants. *J. Chin. Inst. Chem. Eng.* 39: 137–142.

Lee, S.S., Lee, J.Y. and Keener, T.C. (2009a). Mercury oxidation and adsorption characteristics of chemically promoted activated carbon sorbents. *Fuel Process. Technol.* 90: 1314–1318.

Lee, S.S., Lee, J.Y. and Keener, T.C. (2009b). The effect of methods of preparation on the performance of cupric chloride-impregnated sorbents for the removal of mercury from flue gases. *Fuel* 88: 2053–2056.

Lee, S.S., Lee, J.Y. and Keener, T.C. (2009c). Bench-scale studies of in-duct mercury capture using cupric chloride-impregnated carbons. *Environ. Sci. Technol.* 43: 2957–2962.

Li, Q., Jiang, J., Duan, L., Deng, J., Jiang, L., Li, Z. and Hao, J. (2015). Improving the removal efficiency of elemental mercury by pre-existing aerosol particles in double dielectric barrier discharge treatments. *Aerosol*

Air Qual. Res. 15: 1506–1513.

Li, X., Liu, Z., Kim, J. and Lee, J.Y. (2013). Heterogeneous catalytic reaction of elemental mercury vapor over cupric chloride for mercury emissions control. *Appl. Catal., B* 132–133: 401–407.

Li, Y.H., Lee, C.W. and Gullett, B.K. (2003). Importance of activated carbon's oxygen surface functional groups on elemental mercury adsorption. *Fuel* 82: 451–457.

Lippens, B.C. and de Boer, J.H. (1965). Studies on pore systems in catalysts: V. The t method. *J. Catal.* 4: 319–323.

Liu, Z. Li, X., Lee, J.Y. and Bolin, T.B. (2015). Oxidation of elemental mercury vapor over γ-Al_2O_3 supported $CuCl_2$ catalyst for mercury emissions control. *Chem. Eng. J.* 275: 1–7.

Marusczak, N., Castelle, S., de Vogüé, B., Knoery, J. and Cossa, D. (2016). Seasonal variations of total gaseous mercury at a French coastal mediterranean site. *Aerosol Air Qual. Res.* 16: 46–60.

Nguyen-Thanh, D. and Bandosz, T.J. (2005). Activated carbons with metal containing bentonite binders as adsorbents of hydrogen sulfide. *Carbon* 43: 359–367.

Pacyna, E.G., Pacyna, J.M., Sundseth, K., Munthe, J., Kindbom, K., Wilson, S., Steenhuisen, F. and Maxson, P. (2010). Global emission of mercury to the atmosphere from anthropogenic sources in 2005 and projections to 2020. *Atmos. Environ.* 44: 2487–2499.

Padak, B., Brunetti, M., Lewis, A. and Wilcox, J. (2006). Mercury binding on activated carbon. *Environ. Prog.* 25: 319–326.

Skodras, G., Diamantopoulou, Ir., Zabaniotou, A., Stavropoulos, G. and Sakellaropoulos, G.P. (2007). Enhanced mercury adsorption in activated carbons from biomass materials and waste tires. *Fuel Process. Technol.* 88: 749–758.

Skodras, G., Diamantopoulou, Ir., Pantoleontos, G. and Sakellaropoulos, G.P. (2008). Kinetic studies of elemental mercury adsorption in activated carbon fixed bed reactor. *J. Hazard. Mater.* 158: 1–13.

Tseng, H.H. and Wey, M.Y. (2006). Effects of acid treatments of activated carbon on its physiochemical structure as a support for copper oxide in $DeSO_2$ reaction catalysts. *Chemosphere* 62: 756–766.

Vidic, R.D. and Siler, D.P. (2001). Vapor-phase elemental mercury adsorption by activated carbon impregnated with chloride and chelating agents. *Carbon* 39: 3–14.

Vitolo, S. and Seggiani, M. (2002). Mercury removal from geothermal exhaust gas by sulfur-impregnated and virgin activated carbons. *Geothermics* 31: 431–442.

Wang, Y., Shi, L., Chiang, P.C., Mou, X.F. and Liang, H.J. (2016). Emission and species distribution of mercury during thermal treatment of coal fly ash. *Aerosol Air Qual. Res.* 16: 1701–1712.

Wilcox, J., Rupp, E., Ying, S.C., Lim, D.H., Negreira, A.S., Kirchofer, A., Feng, F. and Lee, K. (2012) Mercury adsorption and oxidation in coal combustion and gasification processes. *Int. J. Coal Geol.* 90–91: 4–20.

Williams, N.C. and Petersen, F.W. (1997). The optimisation of an impregnated carbon system to selectively recover cyanide from dilute solutions. *Miner. Eng.* 10: 483–490.

Yang, J., Zhao, Y., Zhang, J. and Zheng, C. (2016a). Removal of elemental mercury from flue gas by recyclable $CuCl_2$ modified magnetospheres catalyst from fly ash. Part 1. Catalyst characterization and performance evaluation. *Fuel* 164: 419–428.

Yang, J., Zhao, Y., Zhang, J. and Zheng, C. (2016b). Removal of elemental mercury from flue gas by recyclable $CuCl_2$ modified magnetospheres catalyst from fly ash. Part 2. Identification of involved reaction mechanism. *Fuel* 167: 366–374.

Yang, J., Zhao, Y., Zhang, J. and Zheng, C. (2016c). Removal of elemental mercury from flue gas by recyclable $CuCl_2$ modified magnetospheres catalyst from fly ash. Part 3. Regeneration performance in realistic flue gas atmosphere. *Fuel* 173: 1–7.

Yang, J., Zhao, Y., Ma, S., Zhu, B., Zhang, J. and Zheng, C. (2016d). Mercury removal by magnetic biochar derived from simultaneous activation and magnetization of sawdust. *Environ. Sci. Technol.* 50: 12040–12047.

Yang, X. and Al-Duri, B. (2005). Kinetic modeling of liquid-phase adsorption of reactive dyes on activated carbon. *J. Colloid Interface Sci.* 287: 25–34.

Zheng, Y., Jensen, A.D., Windelin, C. and Jensen, F. (2012). Dynamic measurement of mercury adsorption and oxidation on activated carbon in simulated cement kiln flue gas. *Fuel* 93: 649–657.

Received for review, October 6, 2016
Revised, February 25, 2017
Accepted, April 5, 2017